Association of AXL and PD-L1 Expression with Clinical Outcomes in Patients with Advanced Renal Cell Carcinoma Treated with PD-1 Blockade

Stéphane Terry, Cécile Dalban, Nathalie Rioux-Leclercq, Julien Adam, Maxime Meylan, Stephanie Buart, Antoine Bougoüin, Alexandra Lespagnol, Frédéric Dugay, Irelka Colina Moreno, et al.

Association of AXL and PD-L1 expression with clinical outcomes in Patients with advanced Renal Cell Carcinomas treated with PD-1 blockade

Stéphane Terry[1*], Cécile Dalban[2], Nathalie Rioux-Leclercq[3], Julien Adam[1], Maxime Meylan[4], Stéphanie Buart[1], Antoine Bougouin[4], Alexandra Lespagnol[5], Frédéric Dugay[6], Irelka Colina Moreno[4], Guillaume Lacroix[4], James B. Lorens[7], Gro Gausdal[8], Wolf H. Fridman[4], Fathia Mami-Chouaib[1], Nathalie Chaput[9,10,11], Benoit Beuselinck[12], Sylvie Chabaud[2], Janice Barros Monteiro[13], Yann Vano[4,14], Bernard Escudier[1,15], Catherine Sautès-Fridman[4], Laurence Albiges[1,15], and Salem Chouaib[1,16*]

[1]INSERM UMR 1186, Integrative Tumour Immunology and Immunotherapy, Gustave Roussy, Fac. de Médecine - Université Paris-Sud, Université Paris-Saclay, 94805 Villejuif, France

[2]Clinical research department - Biostatistics unit, Centre de lutte contre le cancer - Centre Léon Bérard, 69008 Lyon, France

[3]Service Anatomie et Cytologie Pathologiques, CHU Rennes, Univ Rennes, Inserm, EHESP, Irset (Institut de recherche en santé, environnement et travail), UMR_S 1085, 35000 Rennes, France

[4]Centre de Recherche des Cordeliers, INSERM, Sorbonne Université, Université de Paris, Equipe inflammation, complément et cancer, 75006 Paris, France.

[5]Service de Génétique Moléculaire, CHU Rennes, 35000 Rennes, France

[6]Service de Cytogénétique, CHU Rennes, Univ Rennes, Inserm, EHESP, Irset (Institut de recherche en santé, environnement et travail) – UMR_S 1085, 35000 Rennes, France

[7]Department of Biomedicine, Centre for Cancer Biomarkers, Norwegian Centre of Excellence, University of Bergen, Bergen, Norway.

[8]BerGenBio, Bergen, Norway

[9]Laboratory of Immunomonitoring in Oncology, Gustave Roussy Cancer Campus, CNRS-UMS 3655 and INSERM-US23, F-94805 Villejuif, France.

[10]Faculty of Pharmacy, University Paris-Saclay, F-92296 Chatenay-Malabry, France

[11]Laboratory of Genetic Instability and Oncogenesis, UMR CNRS 8200, Gustave Roussy, Université Paris-Saclay, F-94805 Villejuif, France

[12]Department of General Medical Oncology, University Hospitals Leuven, Leuven, Belgium; Laboratory of Experimental Oncology, Department of Oncology, KU Leuven, Leuven, Belgium

[13]Research and development, Unicancer, Paris, France

[14]Medical Oncology, Hôpital Européen Georges Pompidou, Assistance Publique - Hôpitaux de Paris, Université de Paris, 75015 Paris, France

[15]Department of Medical Oncology, Gustave Roussy, 94805 Villejuif, France 14

[16]Thumbay Research Institute for Precision Medicine, Gulf Medical University, Ajman-4184, United Arab Emirates

***Correspondance:** Stéphane Terry, Salem Chouaib, UMR 1186, Integrative Tumor Immunology and Immunotherapy, Gustave Roussy, 39 Camille Desmoulins, 94805 Villejuif Cedex, France. Phone: 33142114577. Emails: stephane.terry@gustaveroussy.fr; salem.chouaib@gustaveroussy.fr

Running Title: AXL and PD-L1 in resistance to Nivolumab in ccRCC

Keywords: clear-cell renal cell carcinoma; immunotherapy; AXL; PD-L1; anti-PD-1;VHL

Word count (Introduction, results, discussion): 3876 (Method Section): 1706

Total number of figures: 5
Total number of Tables:1

Contains supplementary material

References: 50

Disclosure statement:
L. Albiges reports grants from BMS during the conduct of the study; other support from Pfizer, Novartis, BMS, IPSEN, Astellas, MSD, Merck & Co, Janssen, Astra Zeneca, EISAI outside the submitted work. Y. Vano reports personal fees from Bristol Myers Squibb, MSD, Novartis, Ipsen, Janssen, Roche, Sanofi, Astellas, Merck outside the submitted work. G. Gausdal reports to be an employee at BerGenBio ASA. J. Lorens reports personal fees from BerGenBio ASA, outside the submitted work; in addition, J. Lorens has a patent or patent application pending to BerGenBio ASA. J. Adam reports personal fees from MSD and AstraZeneca outside the submitted work. N. Chaput reports support from AstraZeneca, BMS, GSK, Roche, Sanofi, Cytune Pharma, Gilead, outside the submitted work. N. Rioux-Leclercq reports personal fees from Ipsen and BMS outside the submitted work. B. Beuselinck reports grants from BMS and UNICANCER during the conduct of the study; other support from BMS, MSD, Astra Zeneca, Ipsen, and Merck outside the submitted work. No potential conflicts of interest were disclosed by the other authors.

Translational relance:
This is the first study to demonstrate in a sizable cohort of cases that high tumor AXL expression may affect outcomes of patients with advanced clear-cell renal cell carcinoma treated with anti-PD1 therapy. This study also reveals AXL expression is associated with tumor PD-L1 expression and that co-occurrence of PD-L1 positivity and high AXL expression coincides with reduced overall survival in patients treated with PD-1 blockade. This finding may aid in the selection of treatment for advanced RCC patients.

Abstract

A minority of patients currently respond to single agent immune checkpoint blockade (ICB) and strategies to increase response rates are urgently needed. AXL is receptor tyrosine kinase commonly associated with drug-resistance and poor prognosis in many cancer types including in clear-cell renal cell carcinoma (ccRCC). Recent experimental cues in breast, pancreatic and lung cancer models have linked AXL with immune suppression and resistance to antitumor immunity. However, its role in intrinsic and acquired resistance to ICB remains largely unexplored. In this study, tumoral expression of AXL was examined in ccRCC specimens from 316 metastatic patients receiving PD-1 inhibitor, nivolumab, in the GETUG AFU 26 NIVOREN trial after failure of anti-angiogenic therapy. We assessed associations between AXL and patient outcomes following PD-1 blockade, as well as the relationship with various markers including PD-L1, VEGFA, the immune markers CD3, CD8, CD163, CD20, and the mutational status of the tumor suppressor gene *VHL*. Our results show that high AXL expression levels in tumor cells is associated with lower response rates and a trend to shorter progression-free survival following anti-PD-1 treatment. AXL expression was strongly associated with tumor PD-L1 expression, especially in tumors with *VHL* inactivation. Moreover, patients with tumors displaying concomitant PD-L1 expression and high AXL expression had the worst overall survival. Our findings propose AXL as candidate factor of resistance to PD-1 blockade, and provide compelling support for screening both AXL and PD-L1 expression in the management of advanced ccRCC.

INTRODUCTION

Kidney cancer is responsible for about 175000 deaths each year [1]. The most common type of kidney cancer is clear-cell renal cell carcinoma (ccRCC) accounting for 70%-80% of cases. Treatment with immune checkpoint blockade (ICB) has resulted in striking clinical benefits and changes in the management of patients with advanced ccRCC since anti-PD1 (nivolumab) therapy has been approved as second-line treatment for recurrent metastatic diseases, as well as the anti-PD-1 (nivolumab) plus anti-CTLA-4 (ipilimumab) combination approved as first-line treatment for patients with intermediate and high risk metastatic RCC followed by the combination of PD-1 inhibitor with VEGFR TKIs in any risk group in front line [2–5]. Cell surface receptor PD-1 is especially expressed by T lymphocytes, which can prevent T cells from killing tumor target cells upon binding to its ligands PD-L1 and PD-L2, dampening the immune response. Therefore, PD-1 blockade using specific neutralizing antibodies is able to inhibit interaction of PD-1 with its ligands, which may at least partially restore their activity and boost antitumor T-cell immunity. Nevertheless, only a small proportion of patients benefits from these treatments as shown by the low response rate (RR) on one hand, and high rates of disease progression on the other hand, even in initial responders. This illustrates primary and acquired resistances to PD-1 blockade. In an era of progress where anti-PD-1-based combination approaches are expected to increase RR and prolong treatment efficacy [6,7], it is urgent to better define the underlying biology of resistance and response to PD-1 blockade. Thus, new biomarkers and targets that can be easily and routinely inspected in pathological sections might facilitate treatment decisions and give new therapeutic options for metastatic ccRCC (m-ccRCC).

Notably, ccRCC has specific features: 1) In contrast to most tumor types, ccRCC can

be highly infiltrated by CD8+ T cells, but this infiltration is often associated with poor prognosis [8]; 2) RCC has relatively low mutational load and this parameter does not appear to be a good predictor of response to PD-1 blockade [5]; 3) controversies also exist regarding the utility of PD-L1 expression to predict response. Indeed, PD-L1 expression is associated with poor prognosis in RCC, but its value to predict response to PD-1 blockade is still a matter of debate [5,9,10]. Furthermore, genetic alterations in *PBRM1* and *BAP1* genes as well as focal loss in chromosome 10q23.31 have demonstrated interesting properties to estimate patients who are likely to benefit from ICB [11,12]. The *von Hippel-Lindau* (*VHL*) tumor suppressor gene is also altered in a majority of RCC cases. Defects in *VHL* gene include germline or somatic mutations, loss of heterozygosity through chromosomal loss of 3p and promoter hypermethylation [13]. It is often considered that two “hits” must occur to inactivate *VHL*. Thus, a combination of these alterations can cause bi-allelic inactivation of *VHL* in 60-90% of RCC cases leading to a complete loss-of-function (LOF) of *VHL* gene in some cases, whereas in other cases, such function likely remains intact. *VHL* LOF in tumor cells results in chronic accumulation of hypoxia-inducible factors (HIFs) in the cells entering a pseudohypoxic state likely contributing to tumorigenesis, angiogenesis and changes in the tumor microenvironment (TME), in particular *via* induction of the HIF-target gene, *VEGFA*. Recent studies reported clinical benefits for combination of VEGFR TKIs with ICB [5]. However, the impact of the VHL/HIF/VEGF pathway, beyond anti-angiogenic therapy, in regulating refractory responses to ICB remains unclear.

AXL is member of the TAM (TYRO3-AXL-MER) family of receptor tyrosine kinases, which can regulate tumor cell survival, proliferation, migration, angiogenesis, and interactions with TME [14]. AXL has been associated with drug-resistance and poor

prognosis in many cancer types including in RCC [14]. Notably, AXL expression In human RCC has been associated with high risk of relapse after surgery [15], worse clinical outcome in metastatic patients treated with anti-angiogenic agents, as well as epithelial-mesenchymal transition (EMT) features and fibrosis [16]. Recent evidence in breast, pancreatic and lung cancer models have also linked AXL with immune suppression and resistance to antitumor immunity [17–20]. Yet, the role of AXL in resistance to anti-PD1 therapy remains unknown.

In this study, we aimed to elucidate the potential impact of AXL expression on clinical outcomes of patients with advanced RCC following anti-PD1 treatment.

Materials and Methods

Patients and samples

The renal cancer samples have been collected as part of the NIVOREN GETUG-AFU 26 phase II trial assessing the activity and safety of nivolumab (anti-PD1) in 729 patients with m-ccRCC who failed vascular endothelial growth factor–directed therapies (ClinicalTrials.gov identifier: NCT03013335). This trial was conducted by UNICANCER, approved by the human research ethics committee of UNICANCER and conducted in accordance with guidelines from the International Conference on Harmonization and the Declaration of Helsinki. Patients were enrolled across 27 institutions between February 12, 2016 and July 27, 2017. Safety activity data was reported previously [21]**.** The follow-up was censored on January 2019.

As part of a biomarker cohort, 324 archived formalin-fixed paraffin-embedded (FFPE) tumor tissue specimens were retrospectively analyzed by IHC for immune cell profiling (CD3, CD8, PD-L1, CD20, CD163, VEGFA, and AXL). Specimens were mostly obtained prior anti-angiogenic therapy as 1st or 2nd line regimens (comprising

Sunitinib (83.3%), Axitinib (27.5%), Pazopanib (23.8%), Sorafenib (6.5%), Bevacizumab (3.4%), Cabozantinib (0.3%)), or mTOR inhibition (Everolimus 11%). Cases with paraffin block showing less than 40% of tumor or more than 40% of necrosis, or corresponding to another histological subtype (TFE3 translocation RCC, chromophobe RCC or papillary RCC) were excluded.

Alterations in *VHL* gene

VHL inactivation status was determined by PCR, FISH and promoter methylation analysis**.** Evaluation of *VHL* point mutations was evaluated by gene sequencing [22]. The three exons and exon–intron junctions of the *VHL* gene were sequenced on DNA extracted from tumor samples, as described previously [23]. Search for deletion of the *VHL* genomic region was performed by FISH using ZytoLight ® SPEC VHL/CEN3 Dual Color Probe (Zytovision, Germany) reviewed by FD. Promoter hypermethylation of *VHL* was assessed by methylation-specific multiplex ligation-dependent probe amplification as described [23]. Presumably two hits are needed for VHL inactivation to occur. Therefore, tumors were classified in two groups. When biallelic alteration was evidenced, the case was classified in a group with *VHL* inactivation, also referred to as *VHL*-/-. Another group consisted of non-inactivated cases, with no alteration or one allelic alteration, referred to as *VHL* +/+; +/-. A few cases were excluded from this analysis when biallelic or monoallelic alterations could not be ascertained because of non-interpretable results, or when the mutation detected was simply defined as possibly damaging with no clear loss of VHL function.

mRNA extraction and analysis of RNA-Seq datasets from RCC patients

RNA-seq data were available for 83 FFPE cases of the Nivoren cohort [24]. Briefly, archived FFPE samples were retrieved before anti-PD-1 treatment, and upon review of H&E slides, the tissue blocks with the highest tumoral content were selected for further processing. Blank slides were produced with 5 µm thickness and macrodissected to only include tumoral tissue, using a total surface area of 50-1800 mm^2. RNA was extracted using the Maxwell RSC RNA FFPE kit (Promega) according to the manufacturer's instructions. Subsequently cDNA libraries were prepared using the Forward QuantSeq 3' mRNA-Seq Library Prep Kit for Illumina (Lexogen) according to the manufacturer's instructions with 5 µL of RNA as input and 16 PCR cycles. cDNA concentrations and fragment length were measured with the QubitTM dsDNA HS assay (Thermofisher) and Bioanalyzer HS DNA electrophoresis (Agilent). Illumina cBOT was used for clonal cluster generation and RNAseq was performed using the HiSeq 4000 kit (Illumina) according to the manufacturer's instructions. For subsequent survival analysis, samples were classified as AXL high (defined by *AXL* mRNA expression ≥ highest 1/3) or AXL Low (defined by *AXL* mRNA expression ≤ lowest 2/3) in the dataset. Progression Free Survival (PFS) was estimated using the Kaplan-Meier method to explore the impact of AXL the different subsets. For association studies, *VHL* status was determined as above. AXL immunostaining also served to classify tumors as AXL^{high} or $AXL^{neg/low}$, and in this case, RNA-seq data was interrogated to evaluate changes in the expression of known gene expression signatures [25–27].

CheckMate RNA-Seq data, clinical, and genomic information were interrogated from the Braun et al. study [11] for 181 advanced ccRCC treated with anti-PD1 in the CheckMate 009, 010 and CheckMate 025. The CheckMate cohorts consist mostly of previously treated anti-angiogenic-refractory patients. Experimental details including

whole-exome and RNA sequencing analyses have been reported previously [11]. Among the samples with both RNA and genomic information, 93% exhibited loss of chromosome 3p carrying *VHL* gene, and 64% were reported with a point mutation in *VHL*. Cases with at least one WT copy of *VHL* were considered as non-inactivated *VHL* cases, whereas cases with at least two alterations were considered as inactivated. Samples were classified as above with AXL^{high} (defined by *AXL* mRNA expression ≥ highest 1/3) and AXL^{low} cases (defined by *AXL* mRNA expression ≤ lowest 2/3). PFS and OS estimates using the Kaplan-Meier method were generated to explore the impact of AXL in all patients (n=181), *VHL*-inactivated (n=78), or *VHL*-non-inactivated (n=44) subgroups.

Immunohistochemistry

All tumor specimens were centrally reviewed by a genitourinary pathologist (NRL). For each case, one representative archived FFPE tissue block was used for IHC. Primary antibodies to stain for PD-L1 (clone 22C3, Dako), CD8 (clone C8/144B, Dako), VEGF (clone SP28, Spring Bioscience Corp), CD163 (clone 10D6 Diagnostic BioSystem), CD20 (clone L26, Agilent), CD3 (polyclonal rabbit antibody, Agilent) were used according to standard protocols. For PD-L1, AXL, CD8, and VEGF, slides were independently evaluated by a genitourinary pathologist (JA, NRL) blinded to the patients' treatment outcomes. For AXL IHC assessment, epitope retrieval was performed in a citrate buffer pH 7.3 (Diapath) during 30 min in a water bath set to 98°C. Endogenous peroxidase activity was inactivated with 3% hydrogen peroxide for 10 minutes. Blocking was performed with IHC/ISH Super Blocking (Leica biosystems) for one hour at 37°C. The primary antibody (clone C89E7, Cell Signaling Technology), was incubated overnight. Omission of the primary antibody was used

as negative control. A multiplicative H-score (0-300) was calculated as the product of intensity scores and the percentage of stained tumor cells. Representative stainings are shown in **Supplementary Fig. S1**. To note, AXL staining could also be detected in various non-tumor cells, in particular immune cells with morphology evocative of myeloid cells (i.e. monocytes/macrophages/DC) (**Supplementary Fig. S1**). A score of 0-3 was given based on the abundance of AXL^+ immune cells.

Patients were considered with Negative (H-score 0), Low (>0 <=50), or High (>50) AXL tumor expression. H-score > 50 was used as cutoff to discriminate between AXL^{high} and $AXL^{neg/low}$ expression. For PD-L1, VEGF and CD8, stainings were performed using a Discovery XT research instrument (Roche) using standardized protocols. For PD-L1 (anti-PD-L1, clone 22C3, Dako). The % of positive tumor cells was evaluated. % ≥ 1 was used as cutoff to discriminate between PD-L1 TC^{neg} and PD-L1 TC^+ expression. For assessment of PDL1 staining in TILs, a manual semi quantitative 3-point scale was employed with score 0 (no $PDL1^+$ TILs), score 1 (rare and focal $PDL1^+$ TILs), score 2 (several foci of $PDL1^+$ TILS), score 3 (diffuse and numerous $PDL1^+$ TILs). For subsequent analysis, the cutoff ≥ 1 was used to discriminate $PD\text{-}L1^{neg}$ and $PD\text{-}L1^+$ in TILs. CD8 positivity (anti-CD8, clone C8/144B, Dako) in TILs was scored according to the proposal of the International ImmunoOncology Biomarkers Working Group [28], using a manual semi quantitative four point scale : score 0 (no $CD8^+$ TILs or very rare CD8+ TILS), score 1 (rare diffuse or focal $CD8^+$ TILs), score 2 (diffuse numerous $CD8^+$ TILs), and score 3 (diffuse and numerous $CD8^+$ TILs with some aggregates of TILs). Anti-VEGF (clone SP28, Spring Bioscience Corp) was used and the % of positive tumor cells assessed. For CD3 (polyclonal rabbit antibody, Agilent), CD20 (clone L26, Agilent), and CD163 (clone 10D6 Diagnostic BioSystem) immunostaining, tissues were deparaffinized and

rehydrated by successive baths of Clearene (Leica Biosystems, 3803600E) and ethanol gradient (100%, 90%, 70% and 50%). Antigen retrieval was performed with a PT-link (Dako) at pH 6.1 (EnVision FLEX Target Retrieval Solution, Low pH 50x concentrated Citrate buffer, Dako, K8005) by an incubation of 30 minutes at 97°C. 15 minutes of Endogenous Peroxidase block (H2O2 3% Gifrer, 1060351) and 10 minutes of Protein Block (Dako, X0909) reagents were used for alkaline phosphatase and FcR blocking. The primary and secondary antibodies were incubated for 30 minutes respectively. All these markers were processed on an automated immunostainer (AutostainerPlusLink 48, Dako). Secondary antibodies were revealed by Permanent HRP Green (Zytomed Systems, ZUC070-100) for CD3 (10 minutes), High-Def red IHC chromogen (AP) (Enzo, ADI-950-140-0030) for CD20 (5 minutes) and AEC Substrate Kit, Peroxidase HRP: 3-amino-9-ethylcarbazole (Vector Laboratories, SK-4200) for CD163 (23 minutes). The nuclei were counterstained with hematoxylin (Dako, S3301) during 5-7 minutes and slides were scanned with a Nanozoomer (Hamamatsu) after mounting with Ecomount (Biocare, EM897L). For CD20 and CD3, and glycergel Mounting Medium (Dako, C056330-2) for CD163. The density of positive cells/mm² was quantified in the Tumor Core (TC) by two independent analysts (AB, GL) using Halo10 software (Indica labs).

Statistical analysis

Qualitative data are reported by frequency and proportion. The Chi-square and Fisher's exact tests were used to identify associations between biomarkers, status, or groups as categorical variables. Median follow-up is calculated using the reverse Kaplan-Meier method and presented associated with its 95% CI. PFS was defined as the time between treatment initiation and first progression or death, and Overall

Survival (OS) was defined as the time between treatment initiation and death or date of final contact for patients alive. OS and PFS were estimated using the Kaplan-Meier method and were described in terms of median or specific time point estimation in each subgroup, along with the associated two-sided 95% CI for the estimates and were compared with the log-rank test. A multivariate cox regression model was used to estimate the hazard ratio and 95% CI and adjusted for the following baseline characteristics: International Metastatic Renal Cell Carcinoma Database Consortium (IMDC) risk groups, age, sex and number of previous systemic therapies. Objective Response Rate (ORR) as per central radiology review using Response Evaluation Criteria in Solid Tumors (RECIST) version 1.1 and previously described [21]. Quantitative data are reported by means and range. Non-parametric Mann-Whitney U or Kruskal-Wallis test were applied. A value of $p<0.05$ was considered statistically significant, and all p values were two-sided. Data analyses were carried out using GraphPad (GraphPad Prism), Excel (Microsoft Corp) and SAS 9.4 (SAS Institute Inc, Cary, NC).

Results

AXL expression is associated with worse PFS and resistance to anti-PD-1 therapy

AXL tumor cell staining was detectable in 54.4% of cases (172/316) and AXL expression was considered with high expression (H-score >50) in 23.7% of cases (75/316). Population characteristics of patients with AXL^{high} vs $AXL^{neg/low}$ tumors were comparable in terms of gender, age at diagnosis, metastatic features, radiotherapy, IMDC (International Metastatic RCC Database Consortium), or Eastern Cooperative Oncology Group (ECOG) Performance Status (**Table 1**). Median follow-up was 23.5 months (95% CI, 22.6 to 24.0) and median PFS was 4.5 months (95% CI, 2.9 to 5.2). ORR was 25% for the evaluable cases (78/312). In the AXL^{high} group of patients (H-score > 50), median PFS was shorter (2.8 months (95% CI, 2.5 to 4.8)) than in the $AXL^{neg/low}$ group (4.6 months (95% CI, 3.5 to 5.3); p=0.11). Hazard ratio (HR) for disease progression was 1.26 (95%CI, 0.95 to 1.68), and 12-month PFS rates were 21.3% (12.9-31.2) for AXL^{high} compared to 28.6% (23.0-34.4) for the $AXL^{neg/low}$ group (**Fig. 1A**). On multivariate analysis adjusting for age, sex, IMDC and number of previous therapy lines (2 vs >2), high AXL expression was associated with a trend toward reduced PFS (HR = 1.28 (95%CI, 0.96 to 1.71), p=0.098 (**Supplementary Table S1**). The ORR in patients with AXL^{high} tumors was 15.5% (11/71) vs 27.8% (65/234) in patients with $AXL^{neg/low}$ tumors, indicating an inverse association between

AXL expression and response to anti-PD-1 (**Fig. 1A**, p=0.036). For OS, univariate and multivariate analyses indicated no statistical difference (**Fig. 1A** and **Supplementary Table S2**). Additional analysis showed that patients whose tumors exhibited AXL^{low} or AXL^{neg} profiles had similar clinical outcomes and characteristics (**Supplementary Fig. S2A** and **Supplementary Table S3)**. No association was observed between AXL staining in immune cells and OS, PFS or ORR (not shown).

To further explore the link between AXL expression and clinical outcomes, we exploited the RNA-seq data available for a subset of the cases (n=79). Despite the small number of cases, we recapitulated our findings. A higher AXL expression in the specimens tended to be associated with reduced 12-month PFS (p=0.15) and OS rates (p=0.63) (**Fig. 1B**). We then interrogated expression data from the Braun et al. study [11]. This cohort included patients with advanced RCC patients enrolled in CheckMate (CM-009, CM-010 and CM-025 trials) who were treated with an mTOR inhibitor (Everolimus), or nivolumab after progression on at least one prior anti-angiogenic treatment [11]. The potential effect of high AXL expression on survival and ORR was examined in the anti-PD-1 treated arm. High *AXL* expression was associated with worsened OS under anti-PD-1 (HR for death, 1.46; 95% CI, 1.00 to 2.22, P<0.05) (**Fig. 1C**). Median OS was 19.8 months in patients with tumors expressing high levels of *AXL* mRNA vs 35.1 months in cases displaying reduced levels of AXL mRNA. A trend was observed towards shorter PFS under anti-PD-1 blockade and lower ORR in tumors with high *AXL* mRNA expression (19%, 11/58 cases) compared to tumors with low *AXL* expression (24.56%, 28/114), although the differences could not reach statistical significance.

411 Together, these findings suggest that AXL, especially when highly expressed in
412 cancer cells, may be predictor of tumors with reduced response rate and worse
413 progression following PD-1 blockade.
414
415 **AXL expression is associated with increased tumor expression of PD-L1**
416
417 We then explored the TME composition of these tumors by investigating associations
418 between AXL and various markers as assessed by IHC. This included VEGFA, PD-
419 L1 and markers of the most common immune cell populations CD3, CD8 (T cells),
420 CD163 (macrophages) and CD20 (B-cells). PD-L1 tumor cell staining was detected in
421 23.9% (76/317) of evaluable ccRCC cases and PD-L1 on TILs in 58,6% (186/317) of
422 cases. We then stratified cases according to AXL expression and PD-L1 expression
423 status in tumor cells, and tested putative associations between the two markers (**Fig.**
424 **2A**). A significant enrichment of PD-L1 positivity within tumors with AXL^{high} profile
425 was observed (p=0.0031). Moreover, the mean % of PD-L1 positive tumor cells was
426 increased in the AXL^{high} group compared to tumors with $AXL^{neg/low}$ profiles (p=0.0019)
427 (**Fig. 2A** and **Supplementary Fig. S2B**). In contrast, no significant associations were
428 observed between AXL and PD-L1 TIL expression (not shown, p > .99). AXL
429 expression was associated with a greater proportion of tumor cells positive for VEGF
430 (p=0.002) (**Fig. 2B**). We observed a trend toward a higher level of tumor-infiltrating
431 CD8+ T cells in AXL^{high} vs $AXL^{neg/low}$ cases, and no association between AXL and
432 CD3, CD163, CD20 densities in the tumor core (**Figure 2B-C, Supplementary Fig.**
433 **S2B**). RNA-seq data revealed a trend toward greater inflammation (p=0.072),
434 immune suppression (p=0.105), and monocytic lineage (p=0.052) signatures in
435 AXL^{high} tumors (**Fig. 2D**).

High AXL combined with PD-L1 expression is associated with poor survival in patients treated with PD-1 blockade

We set out to determine the extent to which combining AXL and PD-L1 markers would impact on OS under anti-PD-1 treatment (**Fig. 3**). PD-L1 positive staining in tumor cell alone (using cutoff 0;0.5 versus >=1) associated with worse 12-month survival rate (70% (58.6-78.8) versus 77.3 (71.5-82.1)) with HR for death 1.51; log-rank p = 0.02)(**Fig. 3A**). No association was found with PFS (HR = 1.10, p = 0.5) or the ORR (28.6% in PD-L1^{+} vs 23.9% in PD-L1^{neg} subsets)(**Supplementary Fig. S3A**). PD-L1 staining in TILs had limited impact on OS (12-month survival rate 73.3% (66.4-79) vs 78.7 (70.7-84.8)), HR to death 1.34; log-rank p = 0.09), no impact on PFS (p = 0.16), nor on the ORR (25.1% in PD-L1^{+} vs 25% in PD-L1^{neg}) (**Fig. 3B** and **Supplementary Fig. S3B**).

The combination of the two markers AXL and PD-L1 on tumor cells had significant impact on OS since the group of patients whose tumors exhibited both high levels of AXL and PD-L1 tumor cell positivity had the lowest survival rate at 12 months 60.7% (40.4-76.0%), HR to death 1.98 (1.17-3.35), Logrank p = 0.046, compared to the three other groups (AXL$^{neg/low}$/PD-L1^{+} ; AXL$^{neg/low}$/PD-L1^{neg} ;AXL^{high}/PD-L1^{neg})(**Fig. 3A**). On multivariate analysis adjusting for age, sex, IMDC risk groups and number of previous therapy lines (≤2 vs >2), high AXL combined with PD-L1 expression was associated with a trend to reduced OS (HR = 2.01 (95%CI, 1.18-3.44), p=0.084

(**Supplementary Table S5**)). We further interrogated the prognostic value of combining AXL and PD-L1 TC markers specifically in patients with IMDC intermediate-risk/poor-risk RCC. In this setting, a AXL^{high}/$PD\text{-}L1^{+}$ TC profile was associated with the lowest overall survival rate at 12 months 56.0% (34.8-72.7%) and HR to death 2.05 (1.21-3.50), p=0.053 (**Supplementary Fig. S4**).

There was no significant difference between ORR across the different groups (p=0.123), and AXL/PD-L1 TC combination had little if no further influence on PFS compared to AXL alone (**supplementary Fig. S3A**). However, it is noteworthy that the combination of high AXL expression with PD-L1 staining in TILs displayed notable features, with patients in the AXL high/PD-L1+ TIL group showing the worst clinical outcomes particularly in terms of ORR (12%, p=0.04) and PFS, with relatively low PFS rate at 12 months (15.9% (7.0-28.1%), p=0.14) (**Supplementary Fig. S3B**).

We examined the repartition of the different markers in each subgroup, namely, PD-L1 tumor, PD-L1 TIL, VEGF, CD3, CD8, CD163 and CD20. Patients whose tumors were positive for PD-L1 had increased immune cell infiltration. Hence, both AXL^{high} and $AXL^{neg/low}$ cases within the $PD\text{-}L1^{+}$ subset demonstrated high immune cell infiltration compared to $PD\text{-}L1^{neg}$ groups (**Fig. 4A-B**).

These data indicate that AXL and PD-L1 staining can identify a particular group of patients with poor outcomes when receiving anti-PD-1 treatment.

VHL **status does not interfere with clinical outcomes or AXL expression in advanced ccRCC treated with Nivolumab**

Since *VHL* is the most common genetic alteration in RCC, we characterized *VHL* alterations in the ccRCC cases of the NIVOREN cohort. Point mutations were found

in 76.7% (231/301), LOH in 84.1% (254/302), and promoter hypermethylation in 19.1% (27/141) of cases. *VHL* status could be ascertained in 260 cases. 74% of cases (193/260) were found to have a biallelic alteration of *VHL* which supposes LOF of the gene. Among the remaining cases, 7.7% (20/260) presented with no *VHL* alteration (+/+), and 18% (47/260) had one *VHL* alteration (+/-) implying one remaining functional copy. No significant differences in ORR (chi-square p=0.40), PFS (HR 1.00 (0.73-1.37), p=0.98) or OS (0.92 (0.61-1.38), p=0.68) were observed between patients with biallelic *VHL* inactivation ($VHL^{neg/neg}$) and those presenting with at least one unaltered *VHL* copy ($VHL^{+/+}$ and $VHL^{+/neg}$)(**Supplementary Fig. S5A-B**). AXL expression was homogeneously distributed across cases with or without biallelic *VHL* alterations excluding the possibility that AXL expression is dependent on *VHL* status (**Supplementary Fig. S5C).** When stratified based on *VHL* status, a trend was found towards increased PD-L1 positivity in TILs within tumor specimens harboring a $VHL^{neg/neg}$ profile (**Supplementary Fig. S5C**), whereas $VHL^{+/+}$/$VHL^{+/neg}$ tumors tended to be enriched with PD-L1^{+} tumor cells (**Supplementary Fig. S5C**) in line with a previous study [22]. Analysis of the Nivoren RNAseq dataset [24] indicated that $VHL^{+/+}$/$VHL^{+/neg}$ tumors expressed more PD-L1 (p=0.01) and *VHL* mRNAs (p=0.03) (**Supplementary Fig. S5D**). As expected, $VHL^{neg/neg}$ tumors exhibited increased angiogenesis (p=0.02) and hypoxia signatures (p=0.02). $VHL^{+/+}$/$VHL^{+/neg}$ tumors displayed a higher VEGF tumor expression, suggesting a VHL/HIF-independent regulation of VEGF in this group, as previously proposed [29] (**Supplementary Fig. S6A**).Together, this data support that despite similar clinical outcomes under PD-1 blockade, $VHL^{neg/neg}$ and $VHL^{+/+}$/$VHL^{+/neg}$ tumors are biologically different and associated with a distinct microenvironment.

Association between AXL, PD-L1 and survival according to *VHL* status

We then questioned whether AXL staining would yield comparable prognostic and biologic insights in patients with complete inactivation of *VHL* compared to those with a non-inactivated status. We categorized cases into four groups based on AXL expression >50 and the *VHL* status**.** Patients whose tumors exhibited high AXL expression and $VHL^{neg/neg}$ appeared to have the worst median PFS and 12-month PFS compared to cases with $AXL^{neg/low}$ expression within $VHL^{neg/neg}$ subset, though the overall difference was not significant in the log-rank tests comparing the four groups (**Fig. 5A**). In the $VHL^{neg/neg}$ subset, a separation in the PFS curves was evident between AXL^{high} vs $AXL^{neg/low}$ groups after ~5 months and continued to show differences in time as supported by the 12-month PFS rates of 19.6% versus 29.9%, respectively (**Fig. 5A**). In contrast, in the $VHL^{+/+}$/$VHL^{+/neg}$ tumors, there were no signs of such differences. Of note, when interrogating RNAseq data for a subset of patients, a trend in the same direction was observed toward a negative impact for AXL on PFS in the inactivated *VHL* subset but not in the non-inactivated *VHL* subset (**Fig. 5B**). We then conducted a similar analysis using the Checkmate RNA dataset and generated Kaplan–Meier curves for PFS and OS according to tumor *VHL* status. AXL^{high} expression associated with worsened survival (PFS and OS) compared to $AXL^{neg/low}$ in the inactivated *VHL* group (n=78; P=0.05), whereas no difference was observed in patients conserving at least one WT copy of *VHL* in their tumor (n=44; p=0.49) (**Fig. 5C**). Therefore, the influence of AXL on clinical outcomes was mainly apparent in a $VHL^{neg/neg}$ tumors. The results also suggest that both OS and PFS could be impacted by high AXL expression in this setting.

Finally, we sought to examine the putative interaction between AXL and PD-L1 according to tumoral *VHL* status. The enrichment for PD-L1 positivity in AXL^{high} cases

was restricted to *VHL*$^{neg/neg}$ tumors (p=0.0003) and accompanied by a significant increase in the % of PD-L1^{+} tumor cells in AXL^{high} *VHL*$^{neg/neg}$ cases (**Figure 5D**). In *VHL*$^{+/+}$/*VHL*$^{+/neg}$ cases, PD-L1 staining was detected, but the proportion of positive cases was identical in both the AXL$^{neg/low}$ and AXL^{high} groups (p> 0.99). In contrast, the relationship between AXL with VEGF was perceptible in both *VHL*$^{neg/neg}$ and *VHL*$^{+/+}$/*VHL*$^{+/neg}$ subsets (**Supplementary Fig. S6B**)**.** We observed no particular effects of AXL on the immune infiltrate (CD8, CD3, CD163, CD20) in the *VHL*$^{neg/neg}$ and *VHL*$^{+/+}$/*VHL*$^{+/neg}$ specimens(**Supplementary Fig. S6B** and **S6C**).

Discussion

Immunotherapy approaches are increasingly used in clinical practice. Yet many challenges remain to improve efficacy and RR. Most patients exhibit primary or acquired resistance to immunotherapy for reasons that remain unclear. The development of markers predictive for response or resistance is warranted. While recent studies have already shown promising results of immunotherapies as first-line therapy, it will be critical to provide the best appropriate combinatorial therapy for each patient, and this implies the development of tools to capture the unique microenvironment of their tumor.

In this study, patients with ccRCC tumors exhibiting high expression levels of AXL had poorer clinical response (PFS and ORR) after Nivolumab treatment, but not altered OS. The median follow-up in this study was 23.5 months. Outcome measures derive from a still active multicenter phase II study. Extended follow-up should better inform on the impact of AXL on OS. A final analysis at a four-year minimum follow-up

560 is planned. The findings obtained from the analysis of the CheckMate dataset are
561 concordant with a role for AXL on OS.
562 AXL expression was strongly associated with PD-L1 TC positivity on tumor cells, and
563 patients with tumors displaying concomitant PD-L1 TC expression and high AXL
564 expression had the worst OS. We found no significant differences for PFS. Such
565 discordance between PFS and OS should be interpreted with caution since prior
566 work indicates that PFS may not be an ideal predictor of OS in the setting of anti-PD-
567 1 monotherapy [9].
568 The absence of correlation between PD-L1 expression and ICB therapy response in
569 this cohort is interesting. It could be due to possible interference between factors
570 such as AXL and PD-L1 expressed by tumor cells or TILs, or discrepancies in PD-L1
571 expression in different tumor sites. Intriguingly, patients with tumors exhibiting high
572 AXL TC expression and PD-L1 positivity in TILs demonstrated a much lower
573 response rate, suggesting that AXL might play a substantial role in tumors infiltrated
574 with PD-L1 expressing TILs. The combination of AXL and PD-L1 biomarkers could
575 identify various subgroups of patients displaying high or reduced tumor-infiltrating
576 immune cells. The findings support the hypothesis that AXL may be one factor
577 interfering with the predictive value of PD-L1, though it's not clear yet whether such
578 effects could act directly on tumor cells, TILs or indirectly *via* the TME components, a
579 question that should be addressed in future investigations.
580 It will be important to explore the connections between AXL, microenvironment
581 components and therapeutic outcomes in the context of other treatment regimens,
582 namely the anti-PD-1/anti-CTLA4 combination emerging as a standard-of-care first-
583 line therapy option [10,30], anti-PDL1-based combinations used to treat patients with
584 advanced RCCs [5,31,32], as well as anti-PD-1 based combinations integrating

agents targeting AXL such as cabozantinib, expected to target VEGFR2, MET, RET and AXL [5,33]. Recent data have demonstrated activity of cabozantinib after ICB in m-ccRCC [34]. This treatment might enable to overcome the deleterious effects of AXL.

Although AXL expression was not significantly associated with tumor infiltration by macrophages, B or T cells, a broader assessment of the TME and immune checkpoints is required. Our RNA-seq analysis suggested potential interactions between AXL expression and increased inflammation, immune suppression and monocytic lineage signatures. Such analysis likely suffered from the small number of cases analyzed. Studies using sizeable cohorts of patients will be needed to validate these findings. Multiplex IHC or IF approaches would be needed to fully characterize tumor and immune cell infiltrates in this cohort, dissect intratumor heterogeneity, and test potential associations with therapeutic outcomes.

Our analysis is retrospective and has other potential limitations. A number of cases with FFPE block showing <40% of tumor or more than 40% of necrosis were excluded. The archival tumor specimens were often obtained before anti-angiogenic therapy or at an early-stage disease. This is in line with routine clinical practice for treatment decision-making. However, a longitudinal survey with a multiple sampling scheme may be necessary to fully appreciate the TME composition and monitor the influence of previous treatments. Diseases with specific features (e.g, Sarcomatoid, low grade, IMDC favorable-risk groups) also need further investigations, as the current study was limited by the number of cases in these categories. As reported by Boysen et al. [35], we noted a trend toward a greater sarcomatoid differentiation in AXL positive cases (n=25, p=0.09) as well as an enrichment of high grade tumors (Furhman III and IV) in cases with high AXL expression.

Interestingly, AXL association with PD-L1 and worse PFS was observed in tumors harboring *VHL*$^{neg/neg}$ genetic profile, but it has been unclear if this also occurs in those with *VHL*$^{+/+}$/ *VHL*$^{+/neg}$ status where the number of cases was lower. It is postulated that the TME from *VHL*$^{neg/neg}$ tumors differs from those displaying *VHL*$^{+/+}$ or *VHL*$^{+/neg}$. It would be interesting to see if among the identified subgroups, some are enriched for genomic alterations reported with values for predicting anti-PD-1 responsiveness including *BAP1* and *PBRM1* [11]. This could explain, in part, some of the demonstrated effects on PFS, OS or ORR. Previous studies have demonstrated that loss of *PBRM1* functions can accentuate the transcriptional response of HIF in *VHL*$^{neg/neg}$ RCC [36]. We postulate that a molecular link exists between AXL and loss of *PBRM1* in *VHL*$^{neg/neg}$ RCC tumors.

Moreover, tumor cells may have intrinsic characteristics which likely affect the TME. AXL expression has been associated with EMT, epithelial-mesenchymal plasticity, and phenotypic changes of tumor cells in various cancer types [37]. Compelling evidence also exists that differentiation of tumor cells to a more mesenchymal phenotype can greatly influence the TME *via* increased secretion of immunosuppressive substances such as TGF-beta, VEGF, PD-L1 or IL-8 [38–43]. In a lung cancer study, Thompson and colleagues observed that NSCLC tumors displaying a more mesenchymal phenotype had reduced clinical responses to PD-1 blockade. From this work, the investigators derived an EMT/inflammation-based gene expression signature for predicting clinical response of metastatic NSCLC patients [44]. In a cohort of patients with metastatic urothelial cancer treated with nivolumab, Wang et al. found that particularly in patients with T-cell infiltrated tumors, higher EMT/stromal-related gene expression was associated with lower response rates and poor outcomes [45]. Moreover, Chakravarthy et al. showed that an extracellular

matrix (ECM) transcriptional program involving TGF-β signalling and EMT-related genes is associated with worse prognosis in melanoma and bladder cancer patients treated with anti-PD-1 [46]. In melanoma, Hugo and colleagues identified a gene-expression signature associated with innate PD-1 resistance (IPRES) of metastatic melanoma which involves the upregulation of EMT-related factors, including AXL, immunosuppressive cytokines, hypoxia and pro-angiogenic factors [47].

In our survey, AXL staining in immune cells had no prognostic value. However, because the panel of markers analyzed was limited, we cannot exclude the possibility that a particular immune cell subpopulation expressing AXL contributes to anti-PD-1 responsiveness. Others have reported evidence of associations between AXL expressing immune cell populations, and the establishment of an immunosuppressed TME [48–50]. Future studies are warranted to elucidate the interplay between pseudo-hypoxia status, epithelial-mesenchymal plasticity, AXL, microenvironmental changes and their impact on anti-PD-1 responsiveness.

In summary, we identified associations between expression of AXL, PD-L1 expression and *VHL* status in advanced ccRCC which could contribute to disease progression under ICB therapy. Furthermore, we demonstrated that the combined assessment of AXL and PD-L1 expression may be useful to predict outcomes and discriminate patients who are more likely to be resistant or to benefit from anti-PD-1 immunotherapy.

Acknowledgments

This work was supported by INSERM, Université Paris-Saclay, Cancéropôle Ile-de-France, Sorbonne Université, Université de Paris, la Ligue Contre le Cancer

(EL2015.LNCC/SaC to Salem Chouaib), l'Institut National du Cancer and Direction générale de l'offre de soins (grant INCa-DGOS-PRT-K16-181, GETUG-AFU26-Nivoren translational program to Laurence Albiges), CARPEM program of the Sites Intégrés de Recherche sur le Cancer (SIRIC) (to Catherine Sautès-Fridman) and the association pour la recherche en thérapeutiques innovantes en cancérologie (ARTIC). Maxime Meylan received a PhD fellowship from ARTIC. We thank Florence Tantot (Unicancer) for participating to the translational research program, Sophie Ferlicot (Hôpital de Bicêtre, Paris-Sud 11) for providing material in preliminary studies, Laurence Cornevin, Roselyne Viel and Pascale Bellaud (Plateforme H2P2, Biosit, Univ Rennes, F35000 rennes, France) for outstanding technical assistance.

References

1. Bray F, Ferlay J, Soerjomataram I, Siegel RL, Torre LA, Jemal A. Global cancer statistics 2018: GLOBOCAN estimates of incidence and mortality worldwide for 36 cancers in 185 countries. CA: A Cancer Journal for Clinicians. 2018;68:394–424.

2. Rini BI, Plimack ER, Stus V, Gafanov R, Hawkins R, Nosov D, et al. Pembrolizumab plus Axitinib versus Sunitinib for Advanced Renal-Cell Carcinoma. N Engl J Med. 2019;380:1116–27.

3. Motzer R, Alekseev B, Rha S-Y, Porta C, Eto M, Powles T, et al. Lenvatinib plus Pembrolizumab or Everolimus for Advanced Renal Cell Carcinoma. N Engl J Med. 2021;

4. Choueiri TK, Powles T, Burotto M, Escudier B, Bourlon MT, Zurawski B, et al. Nivolumab plus Cabozantinib versus Sunitinib for Advanced Renal-Cell Carcinoma. N Engl J Med. 2021;384:829–41.

5. Xu W, Atkins MB, McDermott DF. Checkpoint inhibitor immunotherapy in kidney cancer. Nat Rev Urol. 2020;17:137–50.

6. Sharma P, Hu-Lieskovan S, Wargo JA, Ribas A. Primary, Adaptive, and Acquired Resistance to Cancer Immunotherapy. Cell. 2017/02/12 ed. 2017;168:707–23.

7. Upadhaya S, Neftelino ST, Hodge JP, Oliva C, Campbell JR, Yu JX. Combinations take centre stage in PD1/PDL1 inhibitor clinical trials. Nat Rev Drug Discov. 2020;

8. Giraldo NA, Becht E, Pages F, Skliris G, Verkarre V, Vano Y, et al. Orchestration and Prognostic Significance of Immune Checkpoints in the Microenvironment of Primary and Metastatic Renal Cell Cancer. Clinical Cancer Research. 2015;21:3031–40.

9. Motzer RJ, Escudier B, McDermott DF, George S, Hammers HJ, Srinivas S, et al. Nivolumab versus Everolimus in Advanced Renal-Cell Carcinoma. N Engl J Med. 2015;373:1803–13.

10. Motzer RJ, Tannir NM, McDermott DF, Arén Frontera O, Melichar B, Choueiri TK, et al. Nivolumab plus Ipilimumab versus Sunitinib in Advanced Renal-Cell Carcinoma. N Engl J Med. 2018;378:1277–90.

11. Braun DA, Hou Y, Bakouny Z, Ficial M, Sant' Angelo M, Forman J, et al. Interplay of somatic alterations and immune infiltration modulates response to PD-1 blockade in advanced clear cell renal cell carcinoma. Nat Med. 2020;26:909–18.

12. Miao D, Margolis CA, Gao W, Voss MH, Li W, Martini DJ, et al. Genomic correlates of response to immune checkpoint therapies in clear cell renal cell carcinoma. Science. 2018;359:801–6.

13. Hsieh JJ, Le VH, Oyama T, Ricketts CJ, Ho TH, Cheng EH. Chromosome 3p Loss-Orchestrated VHL, HIF, and Epigenetic Deregulation in Clear Cell Renal Cell Carcinoma. Journal of Clinical Oncology: Official Journal of the American Society of Clinical Oncology. 2018;JCO2018792549.

14. Schoumacher M, Burbridge M. Key Roles of AXL and MER Receptor Tyrosine Kinases in Resistance to Multiple Anticancer Therapies. Current oncology reports. 2017/03/03 ed. 2017;19:19.

15. Peterfi L, Bjercke T, Yusenko MV, Kovacs G, Banyai D. Cytoplasmic Expression of AXL Is Associated With High Risk of Postoperative Relapse of Conventional Renal Cell Carcinoma. Anticancer Res. 2020;40:3485–9.

16. Landolt L, Eikrem Ø, Strauss P, Scherer A, Lovett DH, Beisland C, et al. Clear Cell Renal Cell Carcinoma is linked to Epithelial-to-Mesenchymal Transition and to Fibrosis. Physiol Rep. 2017;5.

17. Terry S, Abdou A, Engelsen AST, Buart S, Dessen P, Corgnac S, et al. AXL Targeting Overcomes Human Lung Cancer Cell Resistance to NK- and CTL-Mediated Cytotoxicity. Cancer Immunol Res. 2019;7:1789–802.

18. Guo Z, Li Y, Zhang D, Ma J. Axl inhibition induces the antitumor immune response which can be further potentiated by PD-1 blockade in the mouse cancer models. Oncotarget. 2017/11/23 ed. 2017;8:89761–74.

19. Aguilera TA, Rafat M, Castellini L, Shehade H, Kariolis MS, Hui AB, et al. Reprogramming the immunological microenvironment through radiation and targeting Axl. Nature communications. 2016/12/23 ed. 2016;7:13898.

20. Ludwig KF, Du W, Sorrelle NB, Wnuk-Lipinska K, Topalovski M, Toombs JE, et al. Small-Molecule Inhibition of Axl Targets Tumor Immune Suppression and Enhances Chemotherapy in Pancreatic Cancer. Cancer research. 2017/11/29 ed. 2018;78:246–55.

21. Flippot R, Dalban C, Laguerre B, Borchiellini D, Gravis G, Négrier S, et al. Safety and Efficacy of Nivolumab in Brain Metastases From Renal Cell Carcinoma: Results of the GETUG-AFU 26 NIVOREN Multicenter Phase II Study. J Clin Oncol. 2019;37:2008–16.

22. Messai Y, Gad S, Noman MZ, Le Teuff G, Couve S, Janji B, et al. Renal Cell Carcinoma Programmed Death-ligand 1, a New Direct Target of Hypoxia-inducible Factor-2 Alpha, is Regulated by von Hippel-Lindau Gene Mutation Status. Eur Urol. 2016;70:623–32.

735 23. Kammerer-Jacquet SF, Crouzet L, Brunot A, Dagher J, Pladys A, Edeline J, et al.
736 Independent association of PD-L1 expression with noninactivated VHL clear cell renal cell
737 carcinoma-A finding with therapeutic potential. International journal of cancer. 2016/09/14 ed.
738 2017;140:142–8.

739 24. Meylan M, Beuselinck B, Dalban C, Vano Y, Rioux Leclercq N, Sautès-Fridman C, et al.
740 700O Kidney ccRCC immune classification (KIC) enhances the predictive value of T effector
741 (Teff) and angiogenesis (Angio) signatures in response to nivolumab (N). Annals of
742 Oncology. 2020;31:S553.

743 25. McDermott DF, Huseni MA, Atkins MB, Motzer RJ, Rini BI, Escudier B, et al. Clinical
744 activity and molecular correlates of response to atezolizumab alone or in combination with
745 bevacizumab versus sunitinib in renal cell carcinoma. Nature Medicine. Nature Publishing
746 Group; 2018;24:749–57.

747 26. Becht E, Giraldo NA, Lacroix L, Buttard B, Elarouci N, Petitprez F, et al. Estimating
748 the population abundance of tissue-infiltrating immune and stromal cell populations using
749 gene expression. Genome Biol. 2016;17:218.

750 27. Buffa FM, Harris AL, West CM, Miller CJ. Large meta-analysis of multiple cancers reveals
751 a common, compact and highly prognostic hypoxia metagene. Br J Cancer. 2010;102:428–
752 35.

753 28. Hendry S, Salgado R, Gevaert T, Russell PA, John T, Thapa B, et al. Assessing Tumor-
754 infiltrating Lymphocytes in Solid Tumors: A Practical Review for Pathologists and Proposal
755 for a Standardized Method From the International Immunooncology Biomarkers Working
756 Group: Part 1: Assessing the Host Immune Response, TILs in Invasive Breast Carcinoma
757 and Ductal Carcinoma In Situ, Metastatic Tumor Deposits and Areas for Further Research.
758 Adv Anat Pathol. 2017;24:235–51.

759 29. Patard J-J, Rioux-Leclercq N, Masson D, Zerrouki S, Jouan F, Collet N, et al. Absence of
760 VHL gene alteration and high VEGF expression are associated with tumour aggressiveness
761 and poor survival of renal-cell carcinoma. Br J Cancer. 2009;101:1417–24.

762 30. Tannir NM, Signoretti S, Choueiri TK, McDermott DF, Motzer RJ, Flaifel A, et al. Efficacy
763 and Safety of Nivolumab Plus Ipilimumab versus Sunitinib in First-line Treatment of Patients
764 with Advanced Sarcomatoid Renal Cell Carcinoma. Clin Cancer Res. 2020;

765 31. Motzer RJ, Robbins PB, Powles T, Albiges L, Haanen JB, Larkin J, et al. Avelumab plus
766 axitinib versus sunitinib in advanced renal cell carcinoma: biomarker analysis of the phase 3
767 JAVELIN Renal 101 trial. Nat Med. 2020;

768 32. Motzer RJ, Penkov K, Haanen J, Rini B, Albiges L, Campbell MT, et al. Avelumab plus
769 Axitinib versus Sunitinib for Advanced Renal-Cell Carcinoma. N Engl J Med. 2019;380:1103–
770 15.

771 33. Choueiri TK, Kaelin WG. Targeting the HIF2-VEGF axis in renal cell carcinoma. Nat Med.
772 2020;26:1519–30.

773 34. McGregor BA, Lalani A-KA, Xie W, Steinharter JA, E Bakouny Z, Martini DJ, et al. Activity
774 of cabozantinib after immune checkpoint blockade in metastatic clear-cell renal cell
775 carcinoma. Eur J Cancer. 2020;135:203–10.

776 35. Boysen G, Bausch-Fluck D, Thoma CR, Nowicka AM, Stiehl DP, Cima I, et al.
777 Identification and functional characterization of pVHL-dependent cell surface proteins in renal
778 cell carcinoma. Neoplasia. 2012;14:535–46.

779 36. Gao W, Li W, Xiao T, Liu XS, Kaelin WG. Inactivation of the PBRM1 tumor suppressor
780 gene amplifies the HIF-response in VHL $^{-/-}$ clear cell renal carcinoma. Proc Natl Acad Sci
781 USA. 2017;114:1027–32.

782 37. Lotsberg ML, Rayford A, Thiery JP, Belleggia G, Peters SD, Lorens JB, et al. Decoding
783 cancer's camouflage: epithelial-mesenchymal plasticity in resistance to immune checkpoint
784 blockade. CDR [Internet]. 2020 [cited 2020 Nov 1]; Available from:
785 https://cdrjournal.com/article/view/3689

786 38. Terry S, Savagner P, Ortiz-Cuaran S, Mahjoubi L, Saintigny P, Thiery J-P, et al. New
787 insights into the role of EMT in tumor immune escape. Mol Oncol. 2017;11:824–46.

788 39. Lou Y, Diao L, Cuentas ER, Denning WL, Chen L, Fan YH, et al. Epithelial-Mesenchymal
789 Transition Is Associated with a Distinct Tumor Microenvironment Including Elevation of
790 Inflammatory Signals and Multiple Immune Checkpoints in Lung Adenocarcinoma. Clinical
791 cancer research : an official journal of the American Association for Cancer Research.
792 2016/02/07 ed. 2016;22:3630–42.

793 40. Mak MP, Tong P, Diao L, Cardnell RJ, Gibbons DL, William WN, et al. A Patient-Derived,
794 Pan-Cancer EMT Signature Identifies Global Molecular Alterations and Immune Target
795 Enrichment Following Epithelial-to-Mesenchymal Transition. Clinical cancer research : an
796 official journal of the American Association for Cancer Research. 2015/10/01 ed.
797 2016;22:609–20.

798 41. Dongre A, Rashidian M, Reinhardt F, Bagnato A, Keckesova Z, Ploegh HL, et al.
799 Epithelial-to-Mesenchymal Transition Contributes to Immunosuppression in Breast
800 Carcinomas. Cancer Res. 2017;77:3982–9.

801 42. Chen L, Gibbons DL, Goswami S, Cortez MA, Ahn YH, Byers LA, et al. Metastasis is
802 regulated via microRNA-200/ZEB1 axis control of tumour cell PD-L1 expression and
803 intratumoral immunosuppression. Nature communications. 2014/10/29 ed. 2014;5:5241.

804 43. Horn LA, Fousek K, Palena C. Tumor Plasticity and Resistance to Immunotherapy.
805 Trends Cancer. 2020;6:432–41.

806 44. Thompson JC, Hwang W-T, Davis C, Deshpande C, Jeffries S, Rajpurohit Y, et al. Gene
807 signatures of tumor inflammation and epithelial-to-mesenchymal transition (EMT) predict
808 responses to immune checkpoint blockade in lung cancer with high accuracy. Lung Cancer.
809 2020;139:1–8.

810 45. Wang L, Saci A, Szabo PM, Chasalow SD, Castillo-Martin M, Domingo-Domenech J, et
811 al. EMT- and stroma-related gene expression and resistance to PD-1 blockade in urothelial
812 cancer. Nature Communications. Nature Publishing Group; 2018;9:3503.

813 46. Chakravarthy A, Khan L, Bensler NP, Bose P, De Carvalho DD. TGF-β-associated
814 extracellular matrix genes link cancer-associated fibroblasts to immune evasion and
815 immunotherapy failure. Nat Commun. 2018;9:4692.

816 47. Hugo W, Zaretsky JM, Sun L, Song C, Moreno BH, Hu-Lieskovan S, et al. Genomic and
817 Transcriptomic Features of Response to Anti-PD-1 Therapy in Metastatic Melanoma. Cell.
818 2016;165:35–44.

819 48. Rothlin CV, Ghosh S, Zuniga EI, Oldstone MBA, Lemke G. TAM receptors are pleiotropic
820 inhibitors of the innate immune response. Cell. 2007;131:1124–36.

821 49. Maier B, Leader AM, Chen ST, Tung N, Chang C, LeBerichel J, et al. A conserved
822 dendritic-cell regulatory program limits antitumour immunity. Nature. 2020;580:257–62.

823 50. Tanaka M, Siemann DW. Gas6/Axl Signaling Pathway in the Tumor Immune
824 Microenvironment. Cancers (Basel). 2020;12.

825

826

827

Table 1: Patient characteristics

Variables	AXL Tumor cell score [0;50] n=241	AXL Tumor cell score >50 n=75	All Patients n=316	Tests
Age (years)				
N	241	75	316	T-test
Mean (Std)	62.6 (10.9)	61.9 (10.4)	62.4 (10.7)	0.608
Median (min; max)	64.0 (22.0; 87.0)	62.0 (41.0; 86.0)	64.0 (22.0; 87.0)	
Gender				
Male	194 (80.5%)	63 (84.0%)	257 (81.3%)	Chi-2
Female	47 (19.5%)	12 (16.0%)	59 (18.7%)	P = 0.497
IMDC group				
Favorable	42 (17.4%)	12 (16.0%)	54 (17.1%)	Chi-2
Intermediate	142 (58.9%)	49 (65.3%)	191 (60.4%)	P = 0.580
Poor	57 (23.7%)	14 (18.7%)	71 (22.5%)	
ECOG				
Missing	8	3	11	
0 or 1	199 (85.4%)	63 (87.5%)	262 (85.9%)	Chi-2
2 or 3	34 (14.6%)	9 (12.5%)	43 (14.1%)	P = 0.656
M Stage				
Missing	14	5	19	
0	83 (36.6%)	28 (40.0%)	111 (37.4%)	Chi-2
1	59 (26.0%)	20 (28.6%)	79 (26.6%)	P = 0.657
X	85 (37.4%)	22 (31.4%)	107 (36.0%)	
Furhman				
Missing data	7	2	9	
I, II	69 (29.5%)	13 (17.8%)	82 (26.7%)	Chi-2
III, IV	165 (70.5%)	60 (82.2%)	225 (73.3%)	P = 0.049
Brain Metastasis				
Missing	16	3	19	
NO	197 (87.6%)	65 (90.3%)	262 (88.2%)	Chi-2
YES	28 (12.4%)	7 (9.7%)	35 (11.8%)	P = 0.533
Surgery	241 (100%)	75 (100%)	316 (100%)	
Nephrectomy				
NO	9 (3.7%)	3 (4.0%)	12 (3.8%)	Chi-2
YES	232 (96.3%)	72 (96.0%)	304 (96.2%)	P = 0.916
Radiotherapy				
NO	148 (61.4%)	47 (62.7%)	195 (61.7%)	Chi-2
YES	93 (38.6%)	28 (37.3%)	121 (38.3%)	P = 0.845

828

Figure legends

Figure 1 High AXL expression is associated with a trend to shorter PFS and lower ORR in patients with advanced ccRCC treated with Nivolumab. A, Kaplan–Meier survival curves for PFS and OS of RCC patients when stratified according to AXL H-score into two groups, negative/Low]0;50] vs High >50. Corresponding Objective Response Rates, hazard ratios, median PFS (mPFS), and survival estimates at 12 months post-treatment are shown. **B**, Kaplan–Meier PFS and OS curves, and outcome measures deriving from RNA-seq data available for a subset of cases. Nivolumab-treated RCC patients divided into two groups based on a cutoff ≥ highest 1/3 (High) vs ≤ lowest 2/3 (Low) AXL mRNA expression to assess the impact of AXL on survival outcomes. **C**, Kaplan–Meier PFS and OS curves derived from CheckMate RNA-seq data available from the study of Braun [11]. Nivolumab-treated RCC patients were considered and divided into AXL^{high} or AXL^{low} expression groups as in **B**.

Figure 2 AXL is associated with PD-L1 expression. A, Distribution of PD-L1 (% of cases and % of positive cells) in tumors with $AXL^{neg/low}$ vs AXL^{high} profiles. **B** Distribution of VEGF, CD8, CD3, CD163, CD20 expression in $AXL^{Neg/Low}$ versus AXL^{high} cases. **C**, A heatmap is shown to illustrate the biomarker composition across the tumor specimens according to AXL groups. **D**, RNA-Seq-derived expression of various gene signatures in $AXL^{neg/low}$ vs ^{high} cases. Violin plots are shown with box representing the 25th to 75th percentiles and central line representing the median (Mann-Whitney test).

Figure 3 High AXL expression plus PD-L1 TC positivity is associated with worse OS in patients treated with Nivolumab. A, Kaplan-Meier estimates for OS according to PD-L1 TC status (pos/neg), or AXL expression and PD-L1 TC status (four biomarker subgroups). **B**, Kaplan-Meier estimates for OS according to PD-L1 TIL status (pos/neg), or AXL expression and PD-L1 TIL status (four biomarker subgroups).

Figure 4 biomarker distribution across groups stratified based on PD-L1 TC and AXL expression
A, Bar graphs comparing the biomarker composition in the corresponding subgroups. Data are presented as means. Errors bars are s.e.m. Mann-Whitney test. **B**, A heatmap showing the biomarker distribution across the tumor specimens in the indicated subgroups.

Figure 5 AXL association with PD-L1 and outcomes in *VHL*$^{neg/neg}$ and *VHL*$^{+/+}$ /VHL$^{+/neg}$ tumors A, Kaplan–Meier estimates for PFS in patients divided into four groups based on AXL expression and *VHL* status. In the *VHL*$^{neg/neg}$ subset, patients with tumors expressing high levels of AXL (red line) trended to worse PFS compared to those with $AXL^{Null/Low}$ expression (grey line). **B**, Kaplan–Meier PFS curves generated after categorization using RNA-seq data on a subset of cases in VHL-inactivated (*VHL*$^{neg/neg}$) and *VHL* non-inactivated (*VHL*$^{neg/+}$/ *VHL*$^{+/+}$) cases. **C,** Kaplan–Meier estimates for PFS and OS as in B, but using the CheckMate dataset [11]. P values from Log rank tests are shown. **D**, AXL expression associated with PD-L1 TC expression especially in the *VHL*$^{neg/neg}$ tumors. Distribution of PD-L1 (% of

cases and % of positive cells) across the tumor specimens according to the indicated subgroups. Data are presented as means. Errors bars are s.e.m. Chi-square and Mann-Whitney tests were applied.

FIGURE 1

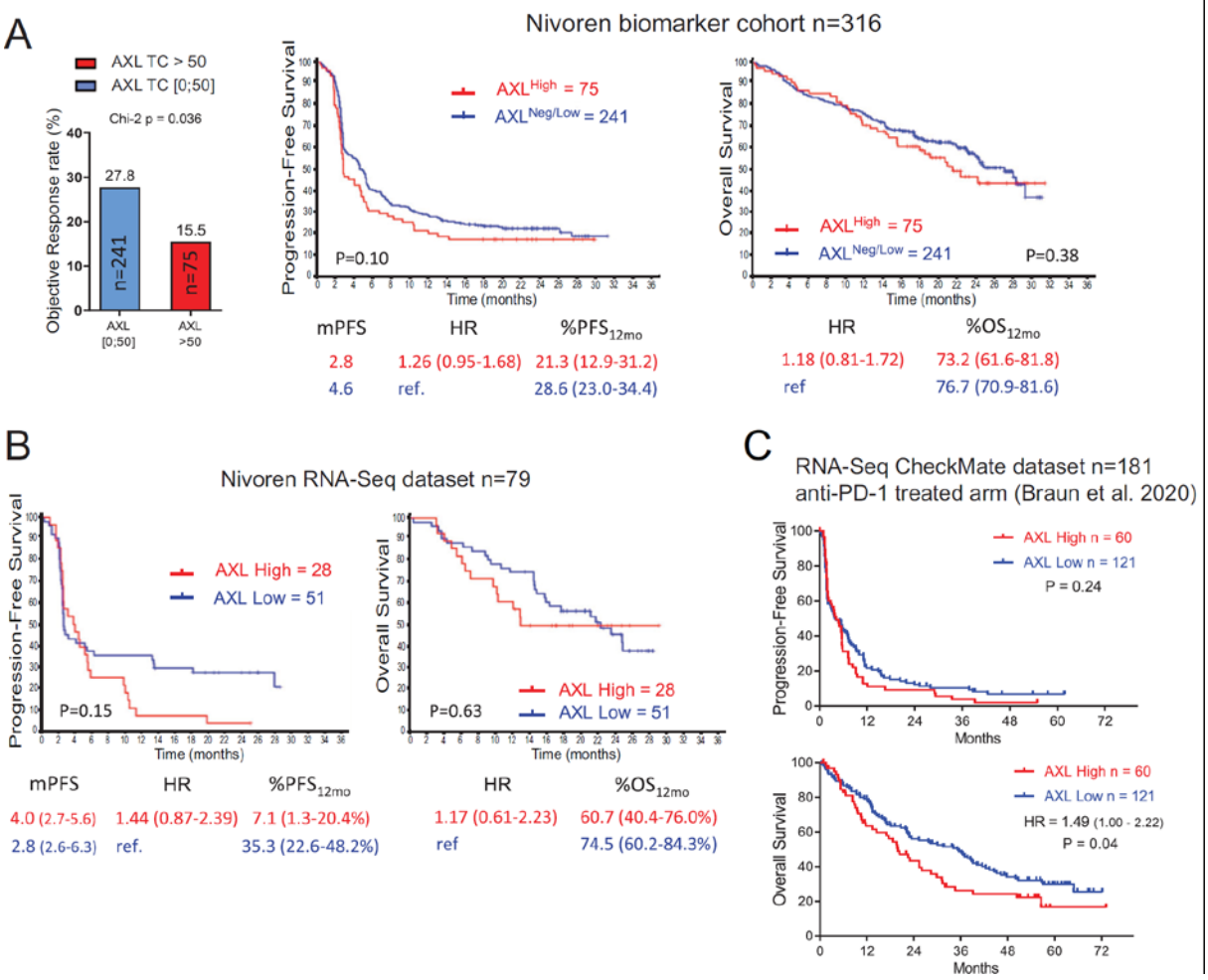

FIGURE 2

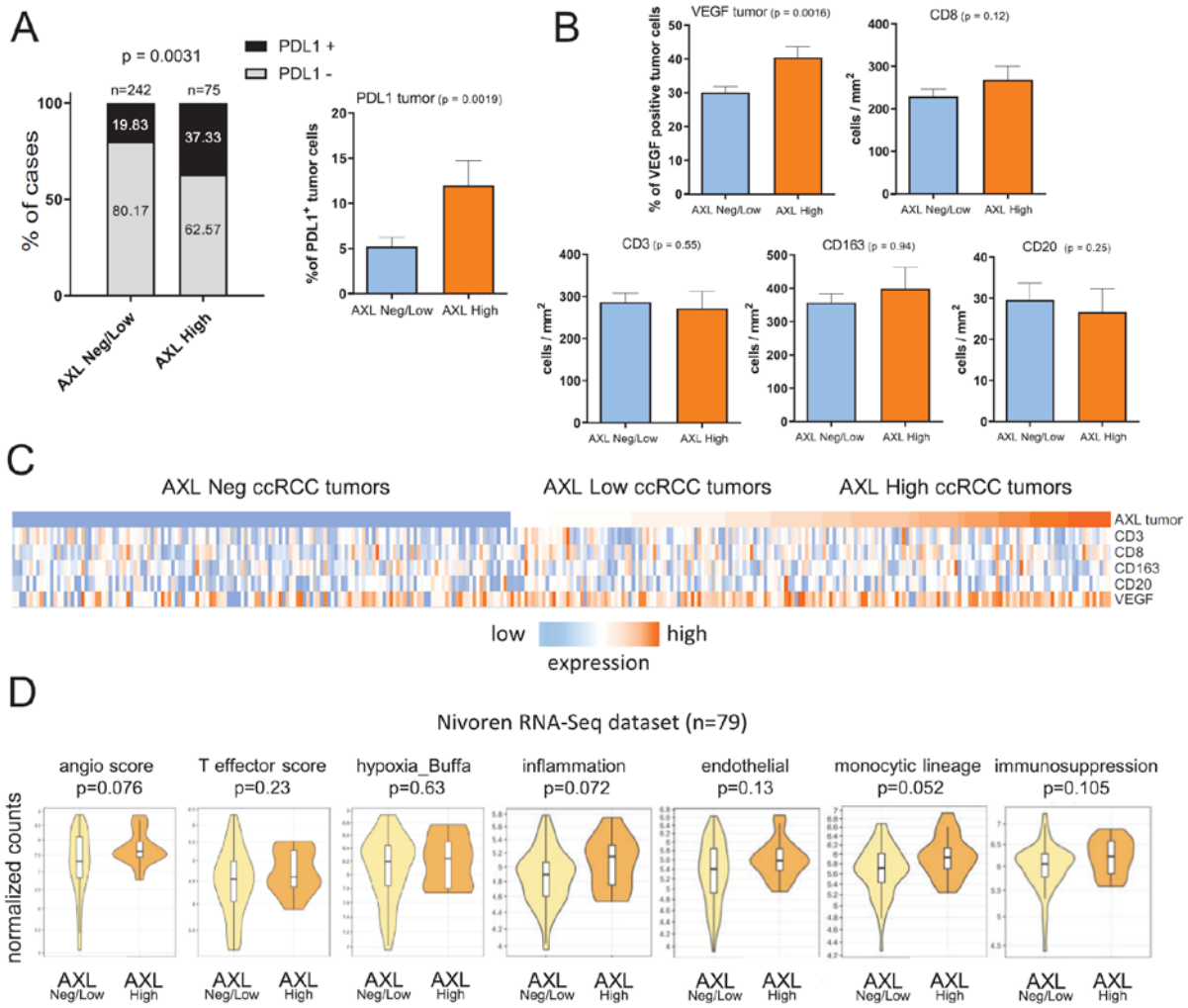

885
886
887

FIGURE 3

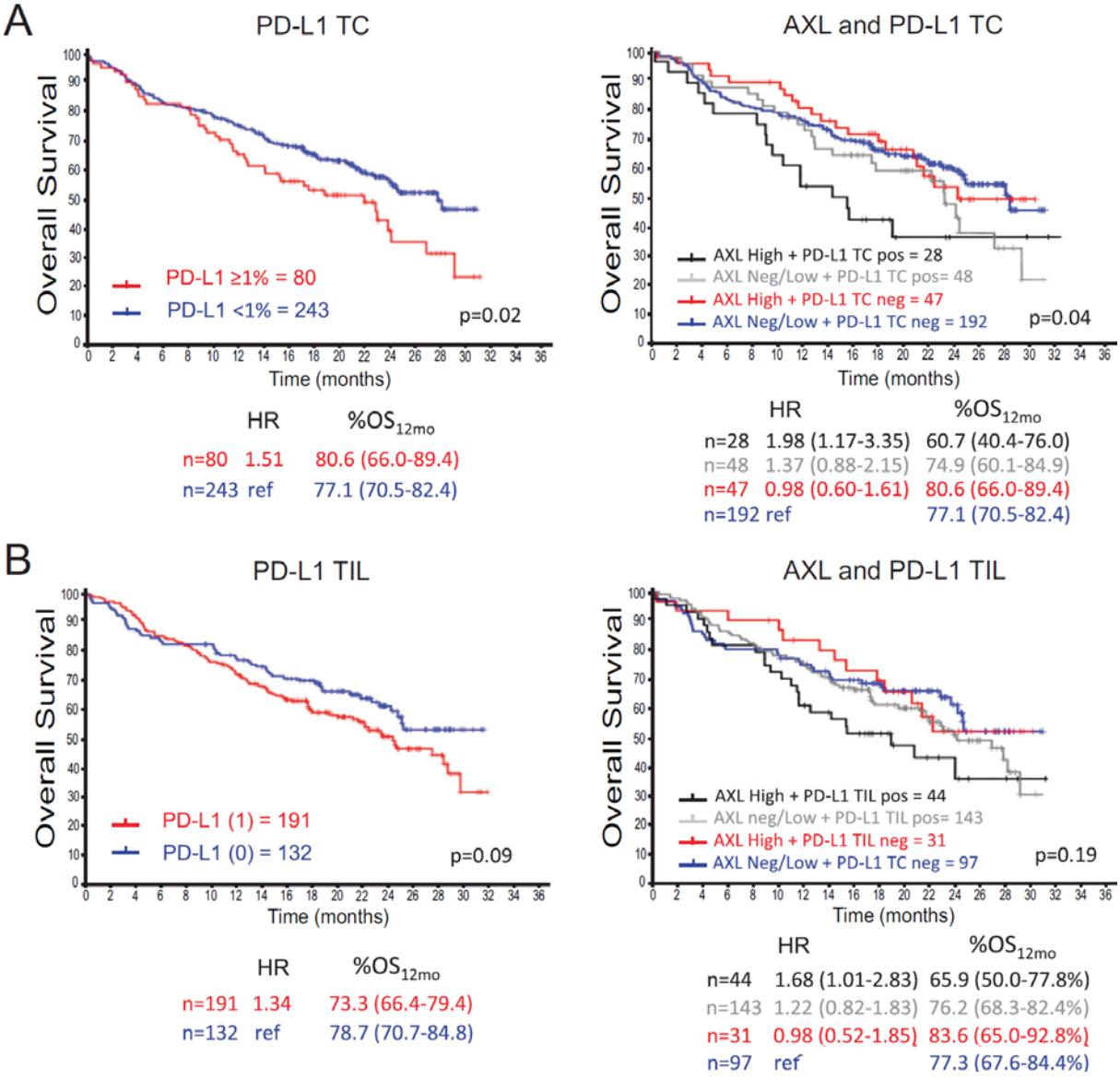

FIGURE 4

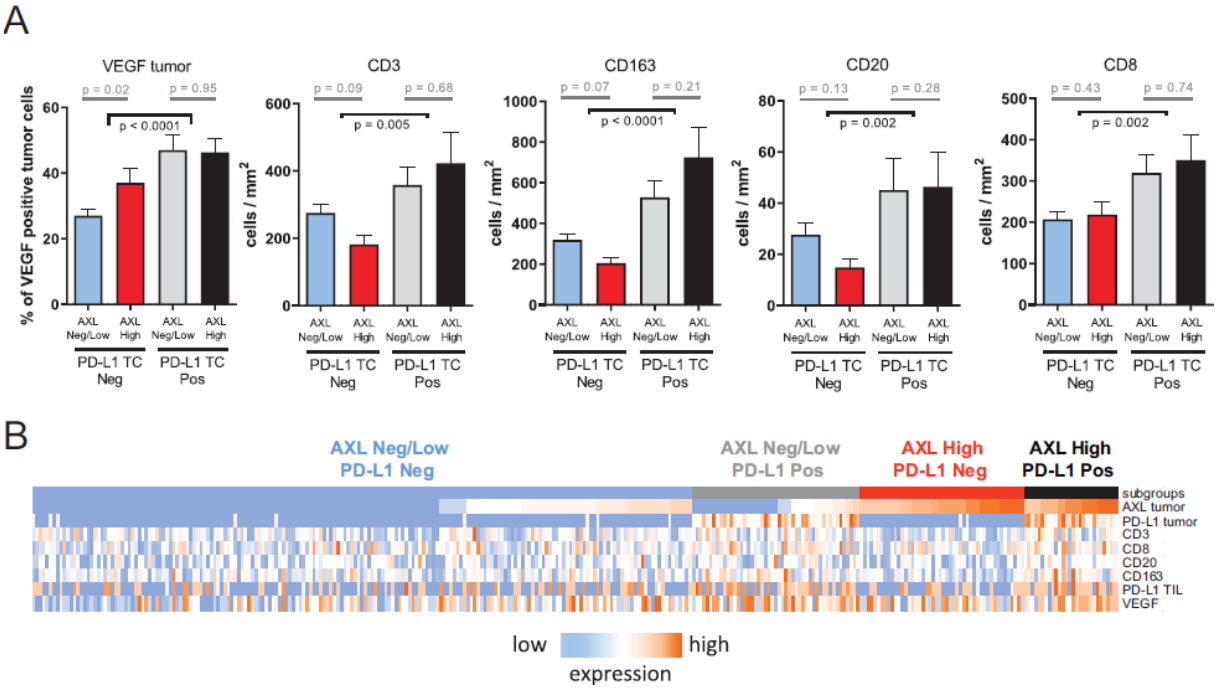

FIGURE 5

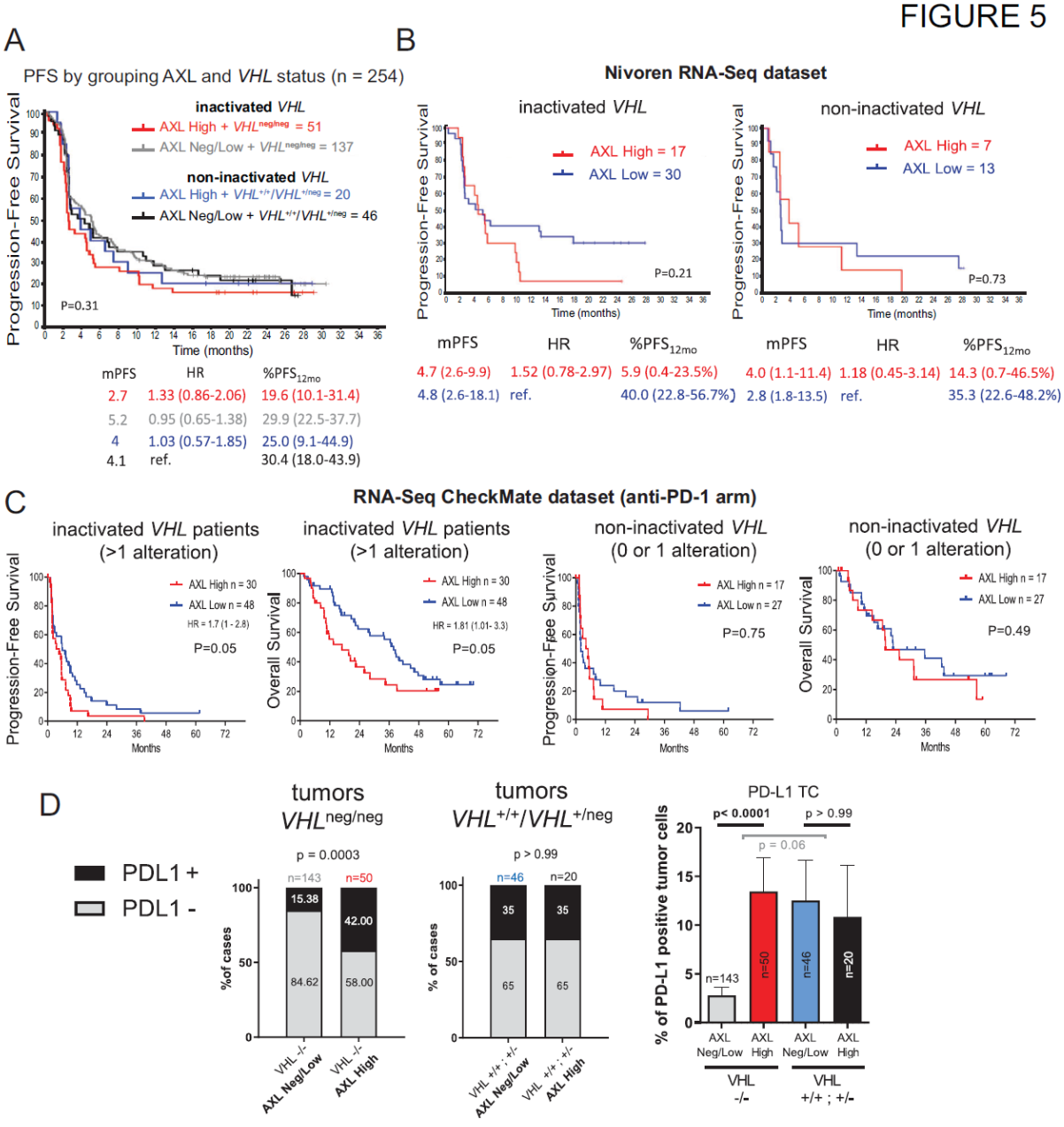

895